Journal of Physics:
Conference Series

Experimental analysis of a graphene oxide-enhanced paraffin PCM

Experimental analysis of a graphene oxide-enhanced paraffin PCM

G Emmi[1], **E Baccega**[1], **S Cesari**[1], **L Giacon**[2], **A Zarrella**[2] **and M Bottarelli**[1]

[1] Department of Architecture, University of Ferrara, Via Quartieri 8, Ferrara, 44121, Italy
[2] Department of Industrial Engineering, University of Padova, Via Venezia 1, Padova, 35131, Italy

Corresponding author: giuseppe.emmi@unife.it

Abstract. The research here presented aims at characterizing the thermal behaviour of a PCM-based latent heat storage enhanced with graphene oxide. The heat storage tank is composed of two PVC coaxial cylinders and a smooth stainless-steel helical heat exchanger installed inside the smaller one. The heat exchanger is immersed in PCM, a commercial paraffin with a melting temperature of around 28°C. The melting and solidification of the PCM were forced through hot or cold water flowing in the heat exchanger. The purpose is to explore the melting and solidification process by monitoring the temperature in the PCM with multiple thermocouples placed at different heights and different radial distances from the centre of the heat exchanger. Initially, the system was studied with pure paraffin. Then, two different mass percentages (i.e., 1.5% and 3%) of graphene oxide were added, whose high thermal conductivity had to counterbalance the paraffin low thermal conductivity and thus enhance the overall performance of the system. These three configurations were then compared to a reference scenario, consisting of the inner cylinder filled with pure water. The use of graphene oxide has increased the heat flux by up to 24% during heating and up to 31% during cooling compared to the pure PCM.

1. Introduction

In recent years the challenge of energy decarbonisation has played a crucial role especially in the field of HVAC in buildings. The most promising way to pursue this goal requires the improvement of the energy performance of the building envelope as well as the reduction of primary energy consumption thanks to the exploitation of renewable energy sources [1-4].

The core of renewable energy systems is represented by the storage. As an example, in case of solar thermal plants or photovoltaic systems, which both need storage to maximize their energy performance and free energy exploitation, the storage is represented by a common buffer tank of technical water or by a battery connected to the system, respectively. As widely known, in fact, the main role of storage systems is to match energy demand and supply even when renewable sources are not available [5-7].

The availability of heat sources and sinks at constant temperatures coupled with high heat capacity is of the outmost importance to guarantee an optimal operation of thermal power plants. However, this result can be obtained only by occupying large spaces for the installation of the plant, which is not always possible as technical rooms do not have enough space.

The adoption of materials with high heat capacity could reduce the size of buffer tanks, thus optimizing and improving the use of the systems powered by renewable energy sources. The materials that currently seem to play a leading role in this field are the so-called Phase Change Materials (PCMs). Energy is

stored in PCMs during the solid–solid, liquid–gas, solid–liquid or solid–gas phase transitions, but in case of thermal power plants the solid-liquid one is the most used.
PCMs can be classified in three different main categories according to their constitution. They can be distinguished into organics, inorganics and eutectics [8]. Organic PCMs have a wide range of thermal properties due to their various molecular structures, which include the hydrocarbon molecules. Part of this category are the so-called paraffins which are the most typical organic PCMs used in energy applications [9]. The second category includes inorganic salts and hydrated inorganic salts. The latter have low melting points if compared to the former, which is the reason why their use is function of the application. The last group of PCMs is represented by mixtures of different substances, named eutectics, which melt or solidify at a single temperature which is lower than each melting temperature of the substances composing the mixture. PCMs, however, present some issues concerning heat transfer and material compatibility. Two ways can be followed to overcome the issues regarding heat transfer, namely work on the material and its thermal properties or work on the heat exchange technology, improving and increasing the heat exchange surfaces between the heat carrier fluid and PCM.
Paraffins are widely studied in literature since they have almost all the characteristics and properties which make them suitable for storage systems, however some strategies to enhance their low thermal conductivity have been suggested and investigated [10]. Aldossary and Sulaiman [11] studied the thermal behaviour of glass with paraffin mixed with CuO nanoparticles by means of simulations, finding the optimal atomic structure for their case study. Similarly, Zhao et al. [12] used molecular dynamics method to study the thermal conductivity of PCM and CuO and results revealed that the thermal conductivity of NPCM is promoted with increasing nanoparticle charges. Yan et al [13] studied a novel erythritol/graphene composite PCM, finding that graphene can not only improve the thermal conductivity of the composites but also reduce the supercooling degree, thus improving the thermal properties of erythritol. Samiyammal et al [14] experimentally investigated the incidence of the mass fraction of magnesium oxide nanoparticles on the thermal properties of paraffin-based PCMs. They found that the blending of 1.0 % of nano-MgO in PCM increase the thermal conductivity by 55.5%, the maximum value obtained during the experimental investigation. Another possibility is to integrate high thermal conductivity materials immersed into the PCM but not on a microscopic scale as in the previous case. This approach leads to an effective thermal conductivity of the PCM. Typical applications in literature involve the use of internal fins, metal foams, carbon fibres and carbon nanotube [15-16]. As an example, the resulting thermal conductivity of paraffin immersed into the metal foams can be increased up to 25 W/(m·K). However, this result is affected by the parameters of metal foams such as porosity, pore density, proportion, and thermal conductivity.
Focus of the research here proposed is the evaluation of the effect of graphene oxide added to a commercial paraffin PCM with the aim of increasing the overall thermal conductivity and thus improving the performance of the newly-enhanced materials when used in a heat exchanger.

2. Methodology

As well stated in the scientific literature, one of the main issues that needs to be addressed when using PCMs is guaranteeing, in addition to a high thermal capacity at the desired temperature, a behaviour that does not affect the performance in terms of heat exchange potential. Indeed, the main drawback of PCMs is their low thermal conductivity, generally in the range of 0.2-0.4W/(m·K) depending on the composition of the material. To overcome this issue, researchers have introduced many technological solutions to improve PCM thermal conductivity. However, these solutions are frequently difficult to integrate or have unsustainable costs, which must be added to the high initial cost of the material itself. In the research here presented, a possible strategy to improve the heat transfer properties of a PCM through the addition of a inert material having a high thermal conductivity was investigated. More specifically, graphene oxide was used, which is easily available on the market and whose cost is relatively low. These aspects would make it potentially affordable and therefore easily accessible for a possible functionalization of the PCM in common heating and cooling applications.
This research was conducted experimentally, by monitoring the thermal behaviour of a small heat storage tank realized *ad hoc* for the purpose, consisting of a helical heat exchanger in which water flows

as heat carrier fluid, immersed in a cylindrical buffer filled with either water, pure PCM or PCM enhanced with graphene oxide.
In this context, the interest was mainly oriented to the evaluation of the behaviour of the PCM and not to the optimization of the heat exchanger used in the experimentation, which is the reason why the exchanger does not have an improved external surface to maximize the surface in contact with the PCM, as described in detail in the following sections.
In order to evaluate the effect of the different buffer fillings, their behaviour in several tests under the same working conditions were compared. These analyses were carried out both in solidification and in melting so that any technological issue that could arise during the two distinct phases could be identified.

2.1. Experimental set up

The heat storage tank used for the tests consists of two coaxial PVC cylinders, 5 mm thick the outer one and 3 mm thick the inner one, with internal diameters of 23 cm and 19 cm, respectively, and a height of 50 cm. Between the two cylinders, an air gap works as insulation. Inside the inner cylinder, the smooth stainless-steel helical heat exchanger was installed, with an external diameter of 18 mm and 9 turns spaced 40 mm apart. The total length of the coil is approximately 3.3 m, while the volume of the inner cylinder is 0.0142 m^3, reduced to 0.0134 m^3 if considering the volume of the coil.
The stainless-steel coil was then connected to a thermostatic bath [17], which allowed to set the desired temperature and flow rate of the inlet water. However, as regards the water flow rate, the thermostatic bath only allows to set different pump speeds, in a range of 40%-100%. Hence, the previously mentioned flow meter was used to ensure the same flow rate during the different tests.
Then, in order to mix the filling thus limiting the temperature stratification, a recirculation circuit was installed: when melted, the PCM is collected at the bottom of the heat exchanger and, through a pump [18], sent back at the top of it. However, when the buffer filling is undergoing the phase change, hence both phases are present at the same time, a solid fraction is present at the bottom of the buffer that prevent the possibility of using the recirculation pump. For this reason, a small submerged pump was added at the top of the heat exchanger, in line with the level of the liquid PCM, so that it was possible to mix the liquid fraction of the material with the aim on increasing the convection and therefore reduce the time for the complete melting of the PCM. The experimental set up is depicted in Figure 1 and Figure 2.

2.2. Data acquisition system

Data were acquired in terms of temperature and flow rates. More specifically, several T-type thermocouples (accuracy: 0.5 K) were used to monitor temperatures inside the heat exchangers at different positions, as depicted in Figure 3 and Figure 4, in addition to those used for inlet and outlet water temperature at the heat exchanger. As regards the flow rate, a digital flow meter (accuracy: 10 l/h) was installed on the return from the heat exchanger to the circulator. All these sensors were connected to a datalogger, in turn connected to a computer to which data were downloaded at regular and customizable timesteps.

2.3. Experimental tests

The PCM used in the study is Rubitherm RT28 [19], a commercial paraffin with a melting temperature of around 27-29°C and a total heat storage capacity (sensible+latent) of around 250 kJ/kg. The thermophysical properties of the material, as stated by the supplier, are reported in Table 1. Despite its lower thermal conductivity and energy storage capacity if compared to hydrated salts, paraffin was chosen because it is much more stable, not corrosive, and it has almost no supercooling and does not segregate when melted.
The effect of the addition of graphene oxide to the PCM was evaluated by comparing the melting and solidification of the pure PCM, used as benchmark, to those of the two enhanced PCMs.

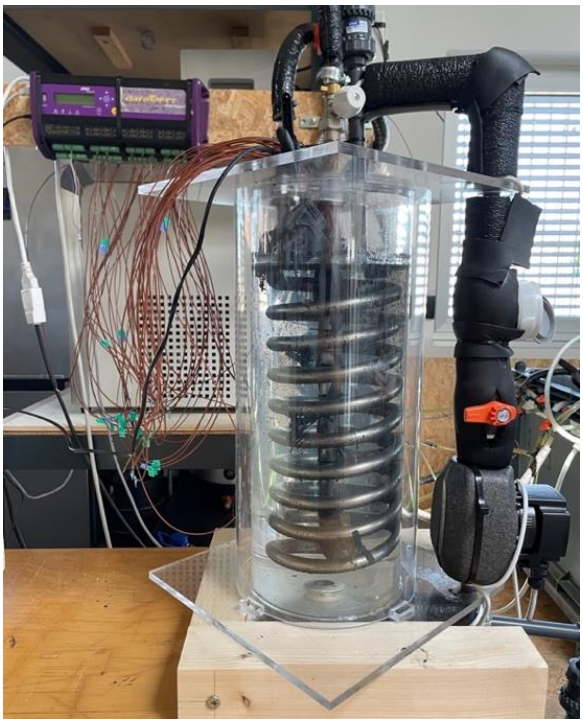

Figure 1. Set up used for the tests. On the right side the recirculation circuit

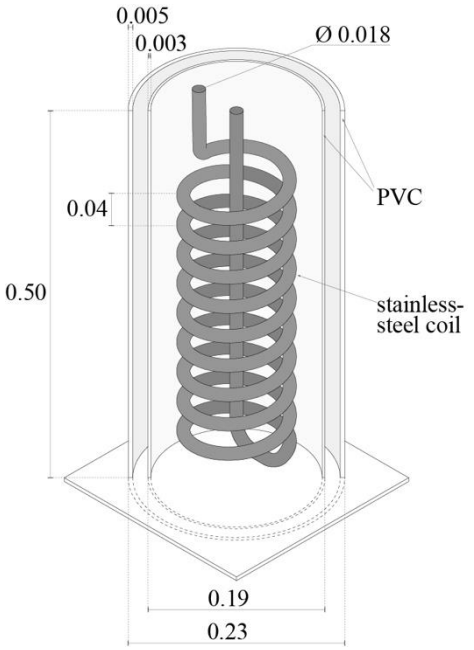

Figure 2. Axonometric view of the set up with main dimensions

Figure 3. Sensors installed close to the coil

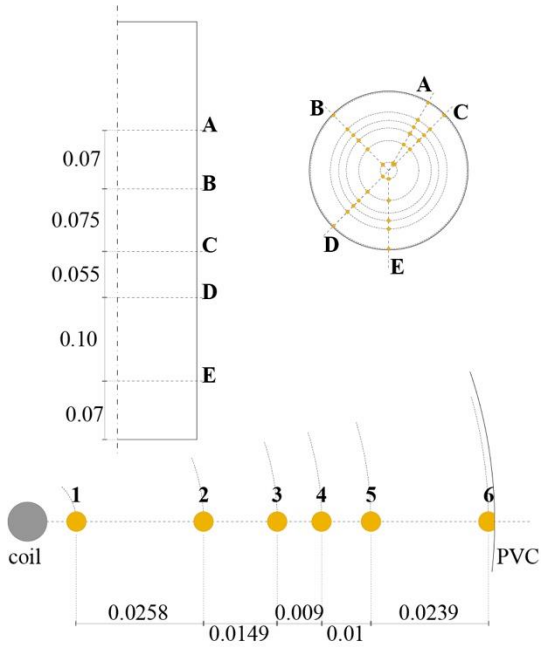

Figure 4. Sensors' position inside the heat exchanger

Table 1. Rubitherm RT28 thermophysical properties

	liquid	solid
ρ [kg/m^3]	770	880
λ [W/(m·K)]	0.2	0.2
c_p [kJ/(kg·K)]	2	2
heat storage capacity [kJ/kg]	250	
phase change range [°C]	27 - 29	

The melting and solidification were monitored during identical tests repeated for the different fillings, the pure RT28 (hereafter renamed PCM), the PCM enhanced with 1.5% by mass of graphene oxide (hereafter renamed 1.5G), and the PCM enhanced with 3.0% by mass of graphene oxide (hereafter renamed 3.0G). Similar tests have been carried out for the pure water. Before starting the tests, the thermal conductivity of the PCM and of the enhanced ones were measured using a HotDisk TPS 1000 [20] and the obtained values are reported in Table 2. It can be noticed that the addition of 1.5% and 3.0% by mass of graphene oxide brought to an increase of 150% and 350% of the paraffin thermal conductivity, respectively.

As regards the melting, the test was carried out by bringing the system to equilibrium at the temperature of 12.3°C, and then by setting the water temperature inside the bath at 45°C. Water was sent into the heat exchanger to heat up the system, until the equilibrium was reached again. During melting, the previously mentioned aquarium pump was turned on, when possible, in order to increase the inner convection and reduce the melting duration.

As regards the solidification, an analogous test was carried out and the entire system was brought at about 45°C by sending hot water to the helical heat exchanger. When reached the equilibrium, the bath was set to 11°C and water started to flow inside the coil, thus cooling down the entire system, and was maintained until the equilibrium was reached again.

Table 2. Measured thermal conductivity of the PCM and the enhanced ones

	PCM	1.5G	3.0G
λ [W/(m·K)]	0.150	0.375	0.680

3. Results and discussion

As mentioned before, the tests were carried out one at a time by maintaining controlled and constant boundary conditions. The room air temperature was constantly monitored during all the tests and values are reported in Figure 5 in case of melting and in Figure 6 in case of solidification. As it can be seen in the charts, during the melting process the temperatures were slightly different each other if compared to the temperatures monitored during the solidification. These small differences affect the heat exchange on the buffer tank envelope. However, the air layer between the two cylinders reduces the magnitude of the phenomenon, making it negligible in any cases.

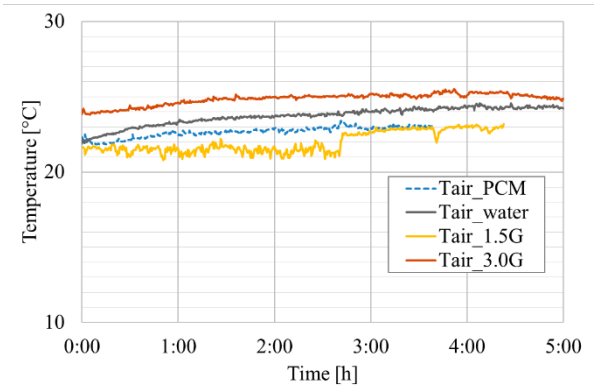

Figure 5. Room air temperature (melting)

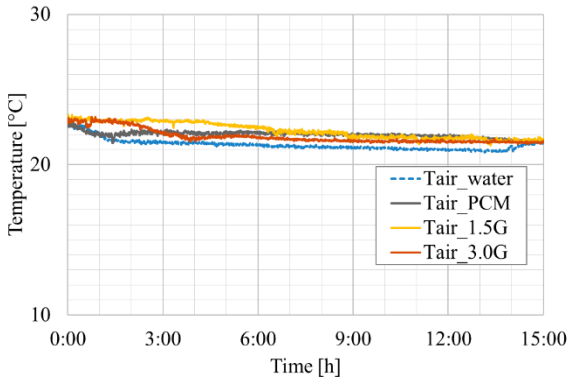

Figure 6. Room air temperature (solidification)

3.1. Melting

As stated before, the PCM has a lower density in liquid form and this keeps the solid fraction of the PCM at the bottom of the buffer tank, phenomenon that can be clearly seen in Figure 7 during the melting process of pure RT28. For this reason, the aquarium pump was turned on during the melting tests to keep the buffer filling mixed, and also to accelerate the transition.

During melting, the system was heated up by running water at 45°C into the coil. The temperature of the thermostatic bath during each of the melting tests is reported in Figure 8, while the differences between inlet temperature, hence that of the bath, and outlet temperature from the coil are reported in Figure 9. Considering the first 30 minutes, a higher difference between inlet and outlet temperatures has been observed for pure water than for PCM or the enhanced PCMs with graphene oxide. After the first 30 minutes, the temperature difference rapidly decreased and became lower. The slight deviation that is visible at 15 minutes corresponds to the moment in which the temperature inside the bath became stable, at 45°C.

Figure 7. Melting process at different timesteps (PCM)

The average values of all the thermocouples installed for each configuration are depicted in Figure 10. As expected, water is the fastest to reach the equilibrium temperature. Differently, as regards the PCM-based buffer fillings, it is evident that at the beginning of the heating up the temperature of 1.5G and 3.0G cases increased at a much higher rate, thanks to the high thermal conductivity of the graphene oxide added. This is better depicted in Figure 11 where the average temperatures in the 1.5G and 3.0G cases are compared to the PCM one. Since the dashed inclined line indicates equal temperatures between the PCM case and the 1.5G and 3.0G cases, it is visible that before the phase change the temperature of the 1.5G and 3.0G cases are always higher than the PCM one, while after the phase change these are almost equal, with differences within the sensors' accuracy.

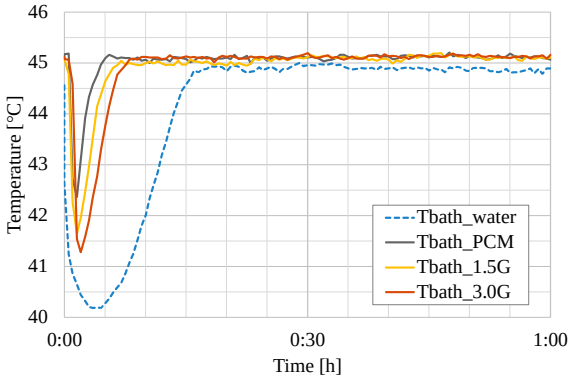

Figure 8. Bath temperature during each test

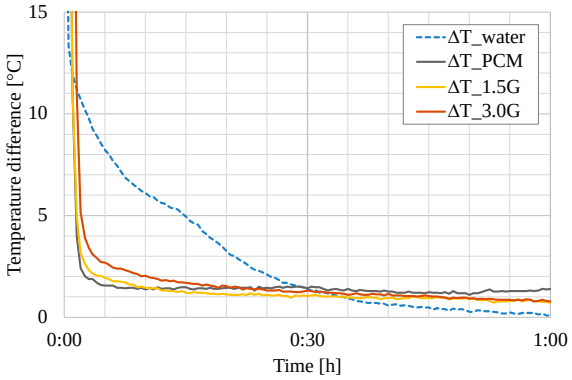

Figure 9. Temperature difference between inlet and outlet during each test

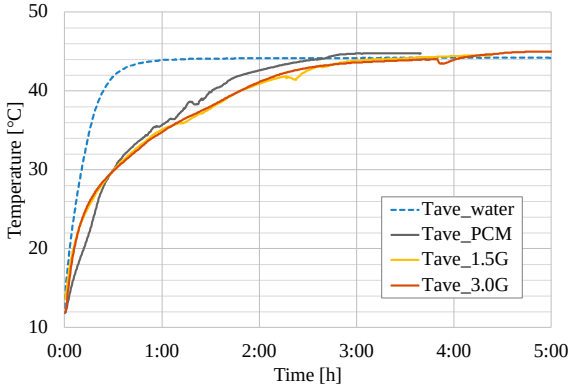

Figure 10. Average temperature in the buffer filling (average of all the thermocouples)

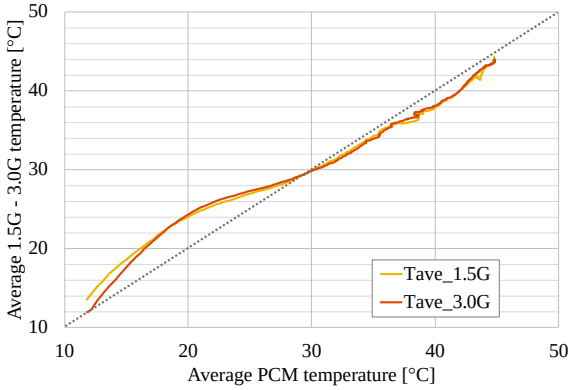

Figure 11. Average temperature in the 1.5G and 3.0 cases compared to the PCM one

As regards the energy exchanged with the buffer filling during the heating up, the cumulative energy calculated for each material is reported in Figure 12. As expected in case of water, since the heat transferred is only sensible, the total energy accumulated is much lower than in case of the PCM or the enhanced ones. As regards the PCM-based buffer fillings, even though the total energy absorbed is almost the same with only slight differences, that might be due to uncertainties of the flow meter and of the thermocouples, their trends are quite different. In the PCM case, hence only pure RT28, the slope is lower than in case of 1.5G and 3.0G, which is due to the lower thermal conductivity. Similarly, in the 3.0G case the energy increased faster thanks to its higher thermal conductivity. These differences can be better noticed in Figure 13, where the instantaneous power for each case is depicted. At the beginning, for the first 30 minutes, the highest power is observed in case of water, followed by the 3.0G, the 1.5G and, at last, the PCM case. From a closer look at the powers in the cases with PCM, it is possible to observe an average improvement of the instantaneous power of 9% and of 24% in the 1.5G and 3.0G, respectively. After the first 30 minutes, the trend is completely reversed, mainly due to the decreasing thermal conductivities that lengthen the overall time. Another observation worth of notice is that in the PCM case the phase change is clearly evident from the almost flat line between 30 and 90 minutes. In the 1.5G the phase change is less visible while in the 3.0G the phase change can be barely seen, both mainly due to the increased thermal conductivity. As it can be seen in the chart, the increase of the thermal power just before one hour on the time scale and just after for the case studies with pure PCM and 1.5G respectively is due to the activation of the immersed small pump. As described before in the text this pump has been installed in the latent heat storage to improve the convective heat exchange on the outer surface of the heat exchanger during the melting process. In the case of 3.0G the pump has not

been activated due to the high viscosity of the mixture of PCM and graphene oxide. The use of a mechanical mixing device would have permitted mixing the contents of the latent heat storage also in this latter case.

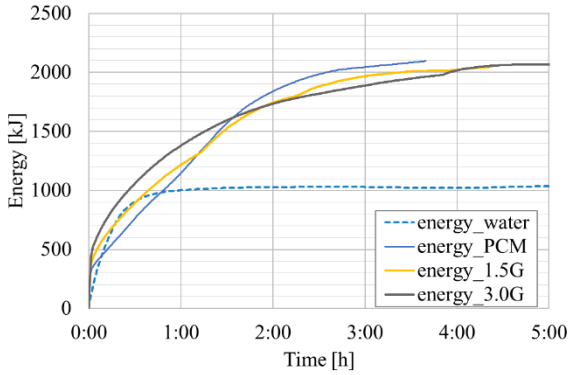

Figure 12. Cumulative energies calculated for each test

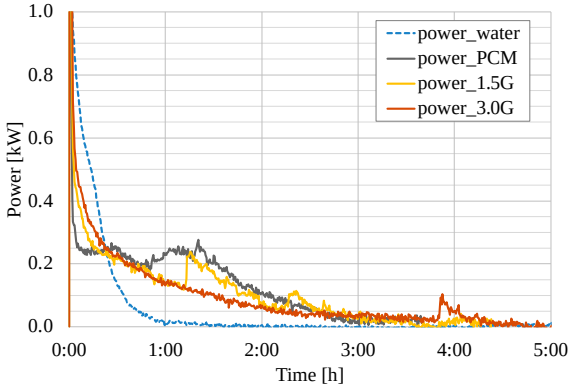

Figure 13. Instantaneous powers calculated for each test

3.2. Solidification

Contrary to melting, the recirculation pump was switched on during the solidification, hence no progressive sedimentation of the solid fraction occurred, as depicted in Figure 14, but rather the phase change started close to the coil and then expanded.

Figure 14. Solidification process at different timesteps (PCM)

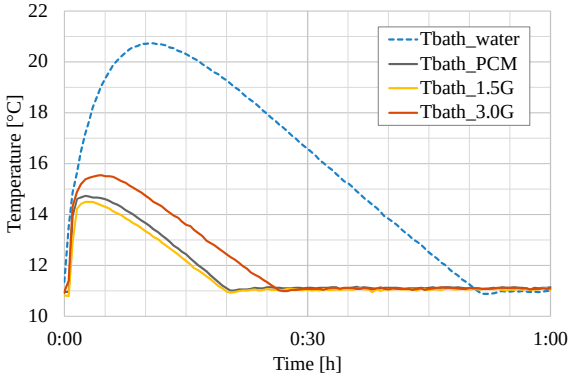

Figure 15. Bath temperature during each test

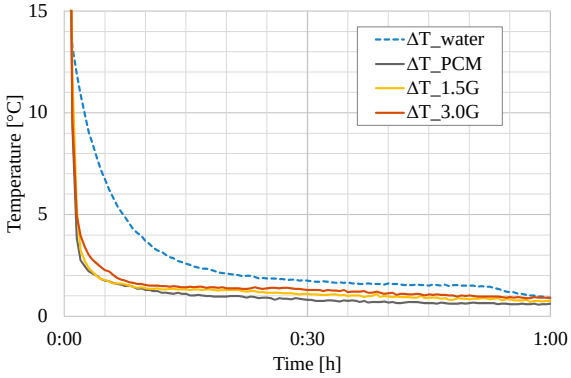

Figure 16. Temperature difference between inlet and outlet during each test

The temperature of the water inside the thermostatic bath is depicted in Figure 15. As observed during melting, in case of water as buffer filling it took much longer to reach the equilibrium, 50 minutes against 20-25 of the PCM-based ones. In terms of temperature differences between inlet and outlet, reported in Figure 16, values for are higher than for the PCM case or the enhanced ones for almost 60 minutes. After this time, differences have smoothed out, becoming barely visible.
As regards temperature inside the heat exchanger, the average values of all the thermocouples installed for each configuration are depicted in Figure 17. As expected, water is the fastest to reach the equilibrium temperature, followed by the 3.0G and the 1.5G cases and, at last, the PCM case. During the cooling process, the differences between the PCM, the 1.5G and 3.0G cases are more visible than during melting, as better depicted in Figure 18, where the average temperatures in the 1.5G and 3.0G cases are compared to the PCM one. During the entire process the temperature in the 1.5G and 3.0G is lower than the PCM, which confirms that the addition of graphene oxide brought to an acceleration of the cooling.
Lastly, as regards the heat exchanged with the buffer filling during the cooling, the cumulative heat calculated for each case is reported in Figure 19. Again, in case of water the total energy accumulated is much lower than in case of the PCM or the enhanced ones. As regards the PCM-based buffer fillings, the most important achievement that can be observed is the velocity of the system: as an example, to reach 1500 kJ the system took 180 minutes in the PCM case, 135 minutes in case of the 1.5G case and 105 minutes in the 3.0G case, with consequent time reductions of 45 and 75 minutes, respectively. The instantaneous calculated powers are depicted in Figure 20, and an improvement of the average instantaneous power of 11% and of 31% in the 1.5G and 3.0G cases can be observed, respectively. After the first 30 minutes, again the trend is completely reversed.

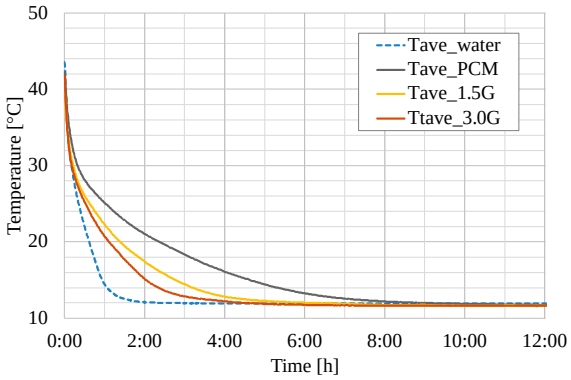

Figure 17. Average temperature at the buffer filling (average of all the thermocouples)

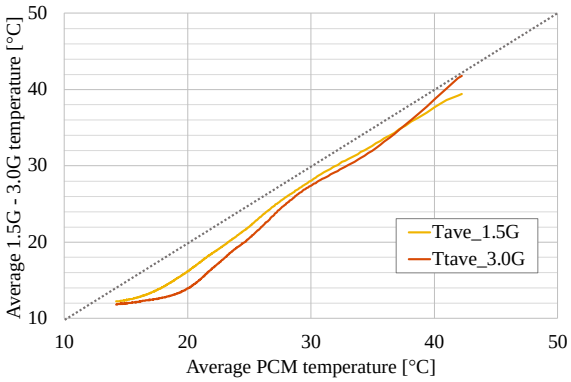

Figure 18. Average temperature in the 1.5G and 3.0 cases compared to the PCM one

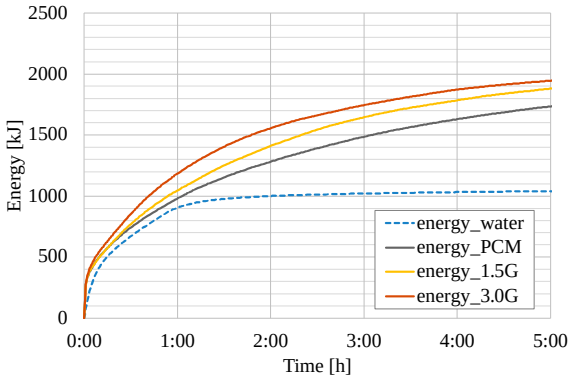

Figure 19. Cumulative energies calculated for each test

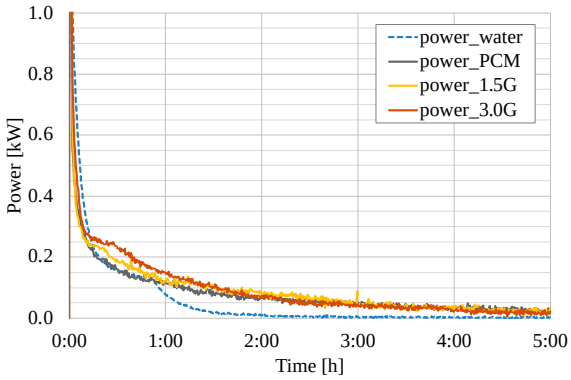

Figure 20. Instantaneous powers calculated for each test

4. Conclusions

Aim of the research here presented is the experimental investigation of the effect of the integration of high thermal conductivity inert inside PCMs in order to increase the overall thermal conductivity, thus improving the overall thermal and energy performance.

The addition of high thermal conductivity graphene oxide into a low thermal conductivity commercial paraffin confirmed that this application is an effective strategy to improve the thermal performance of PCM-based thermal energy storage systems. Results showed that even in small quantities, namely 1.5% and 3% by mass, the graphene oxide could bring to an increase of the thermal conductivity of 150% and 350%, respectively. This also affects the time reduction in reaching the equilibrium temperatures during the heating and cooling tests, with a consequent improvement of the instantaneous power, which resulted to be, in the 1.5G and 3.0G cases, about 9% and 24% higher during heating and 11% and 31% higher during cooling. Considering the same storage volume, the energy accumulated and then released with the application here proposed can be twice the amount of more conventional systems in which water is used as thermal storage.

Further investigations might be focused on other types of PCMs, e.g., hydrated salts, which have a higher thermal conductivity than paraffins and on which the effect of graphene oxide could be even greater. Moreover, further efforts might be concentrated on the improvement of the heat exchanger, in order to increase the exchange available surface and thus reduce the melting and solidification times.

Bibliography

[1] European Commission - Communication from the commission to the European Parliament, the Council, the European Economic and Social Committee and the committee of the regions - A Renovation Wave for Europe - greening our buildings, creating jobs, improving lives, Brussels, 14.10.2020 https://eur-lex.europa.eu/legal-content/EN/TXT/?qid=1603122220757&uri=CELEX:52020DC0662 (Access: 20/05/2023)

[2] Tang B J, Guo Y Y, Yu B and Harvey L D D 2021 Pathways for decarbonizing China's building sector under global warming thresholds *Applied Energy* **298** 117213.

[3] Nägeli C, Jakob M, Catenazzi G and Ostermeyer Y 2020 Policies to decarbonize the Swiss residential building stock: An agent-based building stock modeling assessment *Energy Policy* **146** 111814.

[4] Zhu Q, Leibowicz B D, Busby J W, Shidore S, Adelman D E and Olmstead S M 2022 Enhancing policy realism in energy system optimization models: Politically feasible decarbonization pathways for the United States *Energy Policy* **161** 112754

[5] Zhu X, Zhang X, Gong P and Li Y 2023 A review of distributed energy system optimization for building decarbonization *Journal of Building Engineering* **73** 106735

[6] Cox J L, Hamilton W T and Newman A M 2023 Parametric analysis on optimized design of hybrid solar power plants *Solar Energy* **252** 195–217

[7] Kim D, Wang Z, Brugger J, Blum D, Wetter M, Hong T and Piette M A 2022 Site demonstration and performance evaluation of MPC for a large chiller plant with TES for renewable energy integration and grid decarbonization *Applied Energy* **321** 119343

[8] Cabeza L F 2015 *Advances in Thermal Energy Storage Systems: Methods and Applications* Cabeza L F Woodhead Publishing Series in Energy

[9] Wang X, Li W, Luo Z, Wang K and Shah S P 2022 A critical review on phase change materials (PCM) for sustainable and energy efficient building: Design, characteristic, performance and application Energy *& Buildings* **260** (2022) 111923

[10] Dhaou M H, Mellouli S, Alresheedi F and El-Ghoul Y 2022 Experimental assessment of a solar water tank integrated with nano-enhanced PCM and a stirrer *Alexandria Engineering Journal* **61** 8113–8122

[11] Aldossary A S and Sulaiman N 2022 PCM examine of Silica/Decane nanostructure in the presence of copper oxide nanoparticles to improve the solar energy capacity of glass in the solar collectors via MD approach *Engineering Analysis with Boundary Elements* **145** 72–82

[12] Zhao C Y, Tao Y B and Yu Y S 2022 Thermal conductivity enhancement of phase change material with charged nanoparticle: A molecular dynamics simulation *Energy* **242** 123033
[13] Yan X, Zhao H, Feng Y, Qiu L, Lin L, Zhang X and Ohara T 2022 Excellent heat transfer and phase transformation performance of erythritol/graphene composite phase change materials *Composites Part B* **228** 109435
[14] Samiyammal P, Fuskele V, Fakruddin Babavali S K, Khan N M, Ansari M S and Sakhare D T 2022 Experimental investigations on thermal conductivity and thermal stability of the PCM using Nano- MgO *Materials Today: Proceedings* **69** 759–763
[15] Iasiello M, Mameli M, Filippeschi S and Bianco N 2021 Metal foam/PCM melting evolution analysis: Orientation and morphology effects *Applied Thermal Engineering* **187** 116572
[16] Ding B, Feng W, Mu M, Gong L and Li L 2023 A novel method to concurrently enhance heat conduction and natural convection inside PCM thermal buffer *International Journal of Heat and Mass Transfer* **203** 123773
[17] Thermo Scientific HAAKE PC200 / A25 thermostatic bath https://tools.thermofisher.com/content/sfs/manuals/D00167~.pdf (Access: 20/05/2023)
[18] Grundfos Alpha1L 15-40 130 https://product-selection.grundfos.com/it/products/alpha/alpha1-l/alpha1-l-15-40-130-99160550?tab=variant-curves&pumpsystemid=2133962288 (Access: 20/05/2023)
[19] Rubitherm https://www.rubitherm.eu/media/products/datasheets/Techdata_-RT28HC_EN_09102020.PDF (Access: 20/05/2023)
[20] HotDisk TPS 1000 https://www.hotdiskinstruments.com/products-services/instruments/tps-1000/ (Access: 20/05/2023)